INFLUENCE OF SAMPLE THICKNESS AND CRYSTALLOGRAPHIC ORIENTATION ON THE SIMPLE LANDAU-LIFSHITZ DOMAIN STRUCTURE IN FeSi

By S. Szymura

Institute of Ferrous Metallurgy, Gliwice*

(Received June 30, 1971)

The thickness-dependence of the domain width, $D(T)$, of the simple Landau-Lifshitz domain structure in FeSi is studied for thicknesses ranging from 10^{-3} cm to 1 cm. Rectangular-prism-shaped and wedge-shaped single-crystalline samples are used. The dependence is shown to obey the power-law $D = aT^b$, the crystallographic orientation only affecting the coefficient a. The results obtained with wedge-shaped samples of different wedge angles (up to 90°) are shown to agree very well with those obtained with rectangular-prism samples having faces perpendicular to the crystallographic directions of type ⟨100⟩, provided the former have a symmetric crystallographic orientation. Otherwise, with increasing wedge angle the coefficient a also increases. In rectangular samples with faces parallel to the (110), $(\bar{1}10)$ and (001) planes (Néel cut) the domain structure is found to differ from that predicted by theory.

1. Introduction

Although the Landau-Lifshitz domain structure has been known, thanks to theoretical [1] and experimental studies [2], for a number of years, the first accurate measurements of the domain with D of this structure as a function of crystal thickness T have only relatively recently been performed [3, 4]; these employed single-crystalline FeSi samples cut in the form of wedges. Two different types of Landau-Lifshitz structures, the so-called simple (*SL*) and modified (*ML*) structures, were considered in a range of thicknesses from 10^{-3} cm to 5×10^{-1} cm. It was found that just as for uniaxial Co [5] the $D(T)$ dependence obeys the general power-law

$$D_{X;m} = a_{X;m} T^{b_m} \tag{1}$$

where $m = 1$ or 2, depending on whether the crystal thickness T is smaller or larger than the critical thickness T_0, and the subscript X describes the domain structure type (*e. g.*,

* Address: Zakład Materiałów Magnetycznych, Instytut Metalurgii Żelaza, Gliwice, Miarki 12, Poland.

$X = SL$ or ML for FeSi). It has also been shown that for both types of domain structures examined, the values of T_0, b_1 and b_2 are the same and are $T_0 = 4 \times 10^{-2}$ cm; $b_1 = 0.5$ and $b_2 = 0.9$.

The results of [3, 4] for the ML domain structure have been confirmed in [6] by measurements on a series of single-crystalline FeSi samples in the form of rectangular prisms of various thicknesses and crystallographical orientations. It was found that the results of measurements on samples of simple crystallographic orientation (edges parallel to the [110], [$\bar{1}$10] and [001] directions) coincide with the $D(T)$ dependence found for the ML structure in [3, 4] with the wedge-shaped sample. Moreover, a change in the crystallographic orientation of rectangular-prism-shaped samples only brings a change of the coefficients $a_{ML;m}$ in formula (1) (for $m = 1$ and 2), this alteration being such that the critical thickness T_0 remains unchanged.

Study [7] dealt with the influence of wedge angle and crystallographic orientation of the slanted sides of wedge-shaped samples on the $D(T)$ dependence for the ML domain structure in FeSi. It was shown that for symmetrical wedge-shaped samples (identical crystallographic orientation of the slanted faces) the $D(T)$ curve is idenpendent of the wedge angle and coincides with the results of measurements obtained in [6] for rectangular-prism-shaped samples of simple orientation. It was also ascertained that for non-symmetrical wedge-shaped samples the value of the coefficients $a_{ML;m}$ in formula (1) increases as the sample asymmetry and wedge angle increase, whereas both the critical thickness T_0 and the exponents b_m remain unchanged. In addition, [7] shows that for non-symmetrical wedge-shaped samples the $D(T)$ relationship coincides with the curve in [6] appropriate for rectangular-prism-shaped sample of simple orientation only when the wedge angle is small (less than 20°). This explains the conformity of results of [4] and [6] for the ML domain structure.

The purpose of this work is to examine the SL domain structure in FeSi in an analogous manner as done for the ML structure in [6] and [7]. Another goal is to see if and at what orientation of the rectangular-prism-shaped sample does the SL domain structure transform into the theoretically anticipated domain structure corresponding to the so-called Néel cut [8].

2. *Experimental conditions*

Investigations were carried out with single-crystalline Fe−3.25% Si samples having the form of rectangular prisms and wedges, differing by their crystallographic orientations according to the schematic models in Fig. 1 (angles φ, ϑ and θ). The largest sample thickness t along the magnetically preferred direction was 1 cm, while the width w was 2×10^{-2} cm. The length of the rectangular-prism-shaped samples was always 3 cm; these samples differed from one another by the angle φ (Fig. 1a), which varied within the interval $0 \leqslant \varphi \leqslant 45°$. In the case of the wedge-shaped samples two series of observations and measurements were carried out. The first was performed with symmetrical wedges ($\vartheta = \theta$, Fig. 1b), the wegde angle changing within the interval $0 < \vartheta + \theta \leqslant 90°$. The other series was with the use of non-symmetrical wedges ($\vartheta \neq \theta$), the angle ϑ varying in the interval $0 \leqslant \vartheta \leqslant 45°$ at $\vartheta + \theta = \text{const}$.

The single crystals were obtained from a polycrystalline sheet-metal band by the method of secondary recrystallization described in [9] which resides in pulling the band at a certain speed through a heating device with large temperature gradient. The accuracy in determining the crystallographic orientation of the (100) sides of the samples was ± 10′ (Kris-

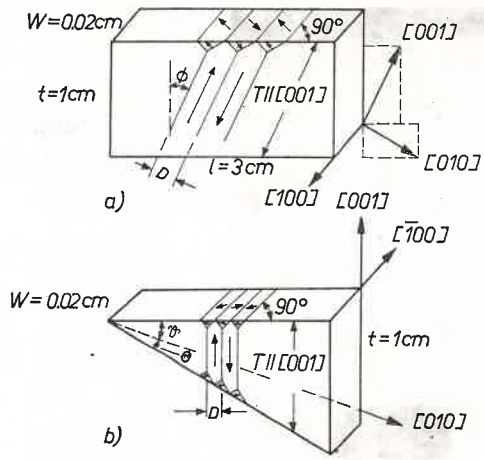

Fig. 1. Shape and crystallographical orientation of samples used in investigations

talloflex 4, Siemens). The mechanical and electrolytic polishing of the samples and the colloid technique used in determining the domain structure were the same as in [2, 10, 11]. For the observations, a Neophot 2 (Zeiss) metallographic microscope was used, and the distance D between the Bloch lines on the (100) surface of the samples, as well as the crystal thickness T and the angles $\varnothing$, ϑ and θ, were determined from averaged measurements on large photographs of the sample and the domain pattern. To account for incidental distortions of the domain structure (local stresses, large vacancies or impurities, *etc.*), the samples were heated to above the Curie temperature and cooled down to room temperature several times and the observations and measurements were repeated. In this way a satisfactory accuracy in determining D, T, $\varnothing$, ϑ and θ has been achieved; for all of these quantities the accuracy was better than 5% for small and 3% for large thicknesses ($T > 10^{-2}$ cm).

3. Results of measurements

3.1. Rectangular-prism-shaped samples

Five series of observations of domain structure and $D(T)$ measurements were carried out on single-crystalline Fe–3.25% Si samples in the form of rectangular prisms cut out as depicted in Fig. 1a. The samples in the various series differed by the angle $\varnothing$, which in succession equalled 0°, 20°, 30°, 40° and 45°.

As was to be expected, the domain structure of the sample corresponding to $\varnothing = 0$ is of the simple Landau-Lifshitz (*SL*) type with closure domains [1]. Figures 2a, b show

the typical powder patterns on the (100) lateral face of such a sample: (a) for $T = 1.28 \times \times 10^{-1}$ cm and (b) for $T = 7.2 \times 10^{-3}$ cm.

The elongation of the closure domains in Fig. 2b at the upper crystal edge is presumably due to local strains which give preference to the [001] easy direction.

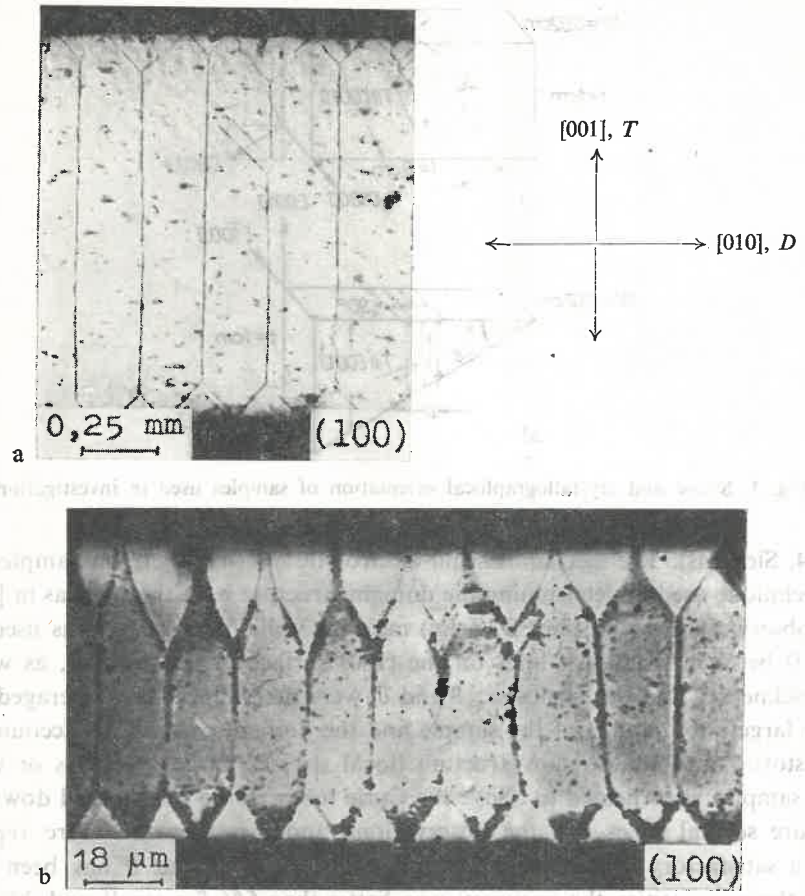

Fig. 2. Powder patterns on (100) lateral face for $\varnothing = 0$ and crystal thickness T in [001] direction: a) 1.28×10^{-1} cm; b) 7.2×10^{-3} cm

Figures 3a, b, c, d show powder patterns of the (100) lateral faces of the samples in Fig. 1 for the respective angles $\varnothing = 20°$, 30°, 40° and 45° and for effective thicknesses $T = 1.1 \times 10^{-1}$ cm, 1.4×10^{-2} cm, 5.25×10^{-2} cm and 8×10^{-2} cm. For the sake of comparison, Fig. 3a (top photograph) also includes the powder patterns of the Bloch line from the upper sample surface corresponding to closure domains visible on the (100) face.

On the basis observations, some examples of which are depicted in Fig. 3, it was established that with an increase of angle $\varnothing$ beyond a certain value ($\sim 25°$) the initial closure domains split up (compare Figs 3a, b, d and the models in Figs 4a, b) or else a different cuneiform type of closure domains appears (Fig. 3c and the model in

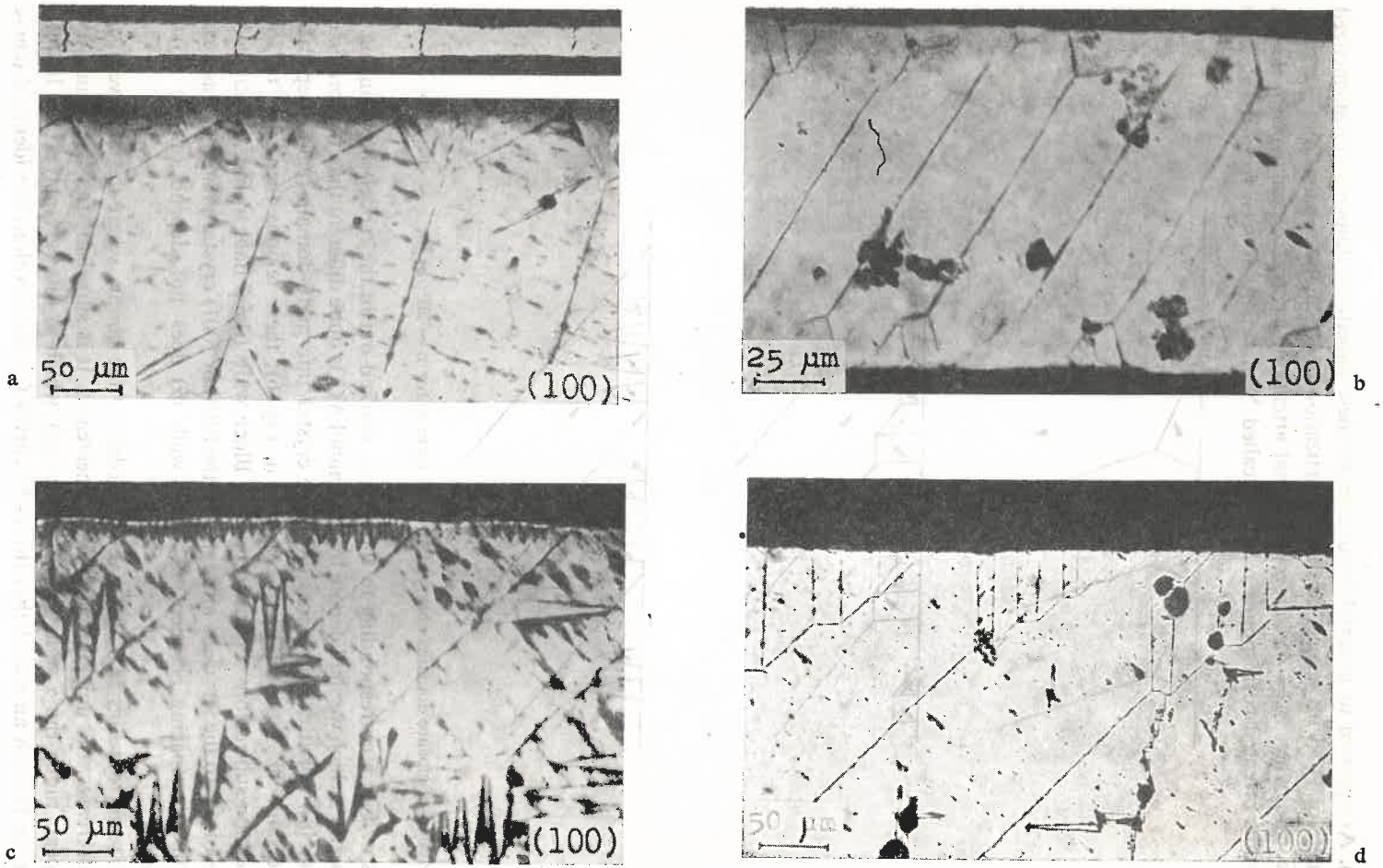

Fig. 3. Powder patterns on (100) lateral face: a) $\varnothing = 20°$ and crystal thickness in [001] direction $T = 1.1 \times 10^{-1}$ cm; b) $\varnothing = 30°$ and $T = 1.4 \times$ $\times 10^{-2}$ cm; c) $\varnothing = 40°$ and $T = 5.25 \times 10^{-2}$ cm; d) $\varnothing = 45°$ and $T = 8 \times 10^{-2}$ cm. The photograph above figure a) shows the powder pattern of the Bloch line at the top sample face corresponding to closure domains on the (100) face

Fig. 4c). As opposed to uniaxial ferromagnets, these cuneiform domains are magnetized at an angle of 90° with respect to the magnetization of the main domains.

The case when $\varnothing = 45°$ deserves special attention, as a rectangular-prism-shaped sample thus oriented corresponds to the so-called Néel cut. As is seen from the powder

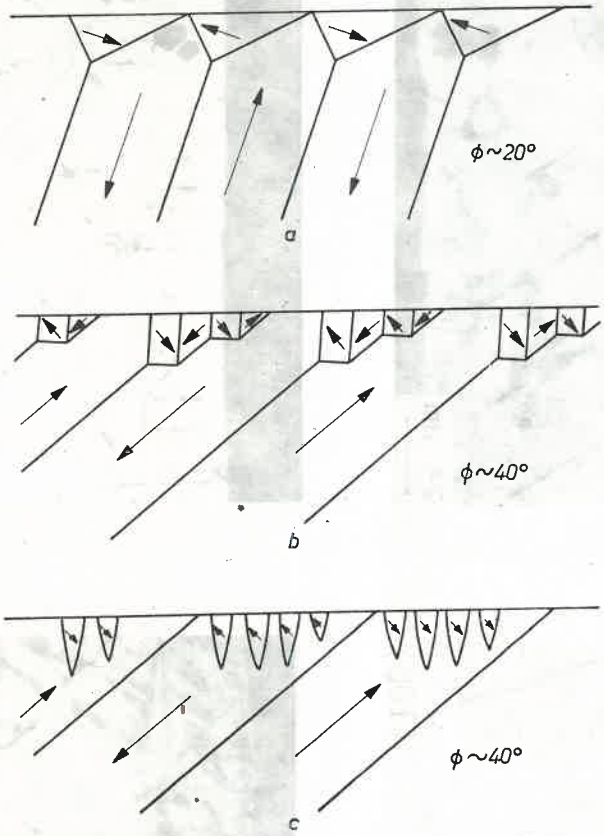

Fig. 4. Models of closure domains observed on (100) face: a) for $\varnothing \sim 20°$; b) for $\varnothing \sim 40°$; c) for $\varnothing \sim 40°$

patterns of Fig. 5 corresponding to the regions marked out in the model shown in Fig. 6 this structure, which we shall denote by the symbol *NC*, is quite different than that predicted by theory [8]. For it exhibits division of the crystal into multi-domain regions separated by equidistant 90° Bloch walls (the α lines in Fig. 6); these regions then split up into single-domain sub-regions separated by 180° Bloch walls (the β lines in Fig. 6) inclined at an angle of 45° to the 90° walls and lying in the (010) or (001) crystal planes. It was ascertained that the spacing between 90° Bloch walls (α) does not depend on the crystal thickness t.

It is seen from Figs 5a and 6 that at the edges of the sample, where the effective thickness T decreases, the domain width D also decreases. It is surprising that the same effect also appears along the α walls (compare Fig. 5d), which in this case play a role like the crystal edge to such an extent that the $D(T)$ curves for these regions are identical (curve

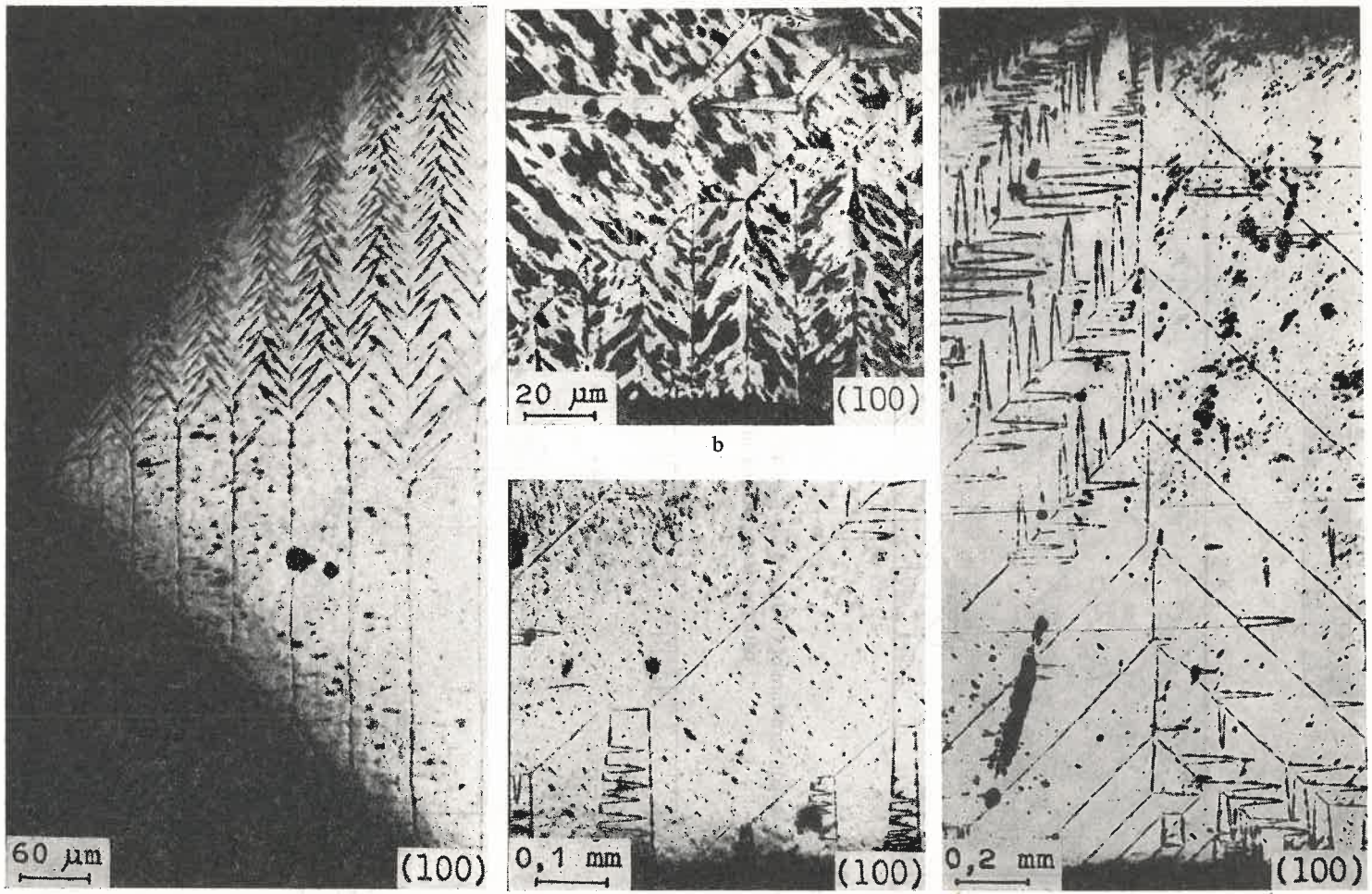

a b c d

Fig. 5. Powder patterns on (100) lateral face of rectangular-prism-shaped sample for $\varphi = 45°$: a) domains at sample edge; b) closure domainsat sample edge; c) equidistant 180° Bloch walls; d) 90° Bloch wall

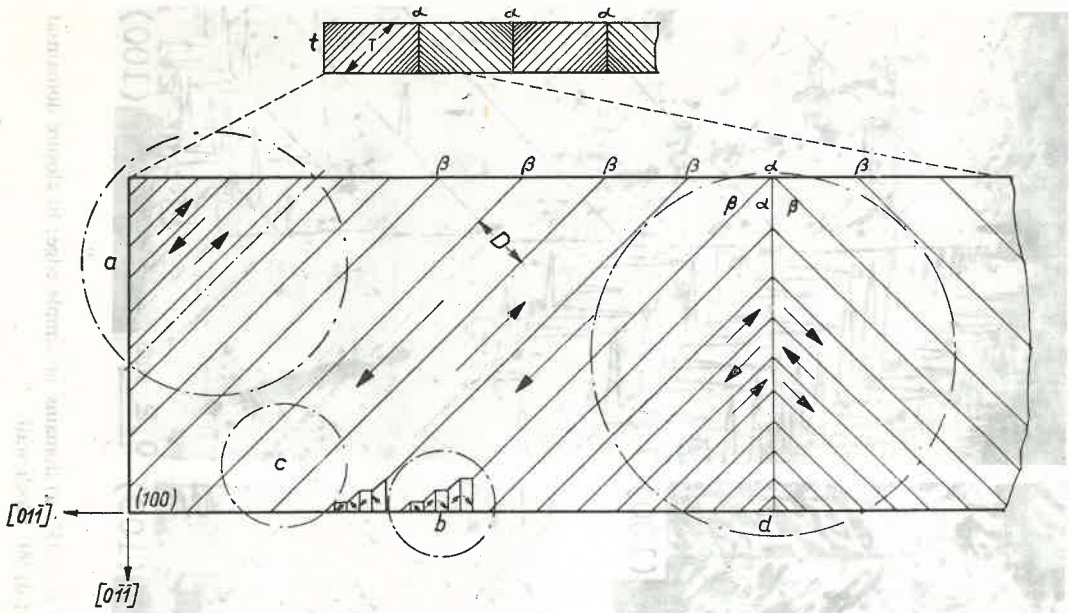

Fig. 6. Model of domain structure of (100) face for $\varphi = 45°$. The circles mark regions for which powder patterns are presented in Fig. 5

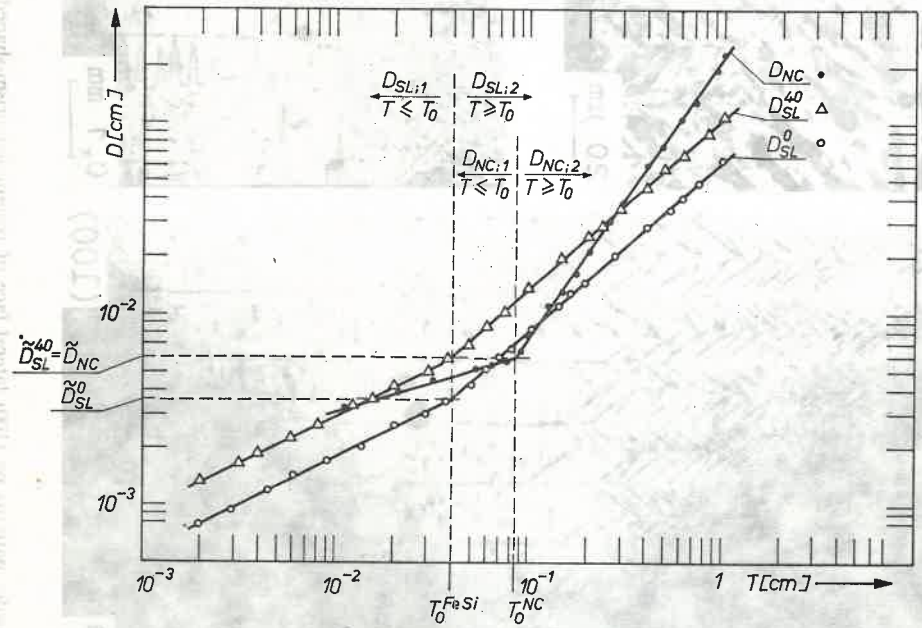

Fig. 7. Domain width D *versus* crystal thickness T for simple domain structure of single-crystalline Fe–3.25% Si samples in the shape of rectangular prisms for: $\varphi = 0°$ (curve D_{SL}^{0}), $\varphi = 40°$ (curve D_{SL}^{40}), $\varphi = 45°$ (curve D_{NC})

D_{NC} in Fig. 7). They are, however, essentially different (dissimilar b_1, b_2 and T_0) than the $D(T)$ curves for the SL structure at $0 \leqslant \varnothing \leqslant 45°$ (Figs 2 and 3), which we denote by the symbol D_{SL}; by way of illustration two such curves, for $\varnothing = 0$ and $\varnothing = 40°$, are given in Fig. 7.

More accurate readings taken from the large plots of the D^0_{SL}, D^{20}_{SL}, D^{30}_{SL} and D^{40}_{SL} curves for the SL domain structure give the following values for the exponents b_m and coefficients $a_{X;m}$ defined by formula (1):

$$a^0_{SL;1} = 0.0183, \quad a^{20}_{SL;1} = 0.0220$$

$b_1 = 0.5$

$$a^{30}_{SL;} = 0.0265, \quad a^{40}_{SL;1} = 0.030 \tag{2}$$

for $m = 1\ (T \leqslant T_0)$, and

$$a^0_{SL;2} = 0.064, \quad a^{20}_{SL;2} = 0.076$$

$b_2 = 0.9$

$$a^{30}_{SL;2} = 0.093, \quad a^{40}_{SL;2} = 0.110 \tag{3}$$

for $m = 2\ (T \geqslant T_0)$, where the coefficients $a^{\varnothing}_{SL;m}$ are measured in units of cm^{1-b_m}. The critical thickness T_0 can be determined immediately from the plot or from the obvious equality

$$a^{\varnothing}_{X;1} T_0^{b_1} = a^{\varnothing}_{X;2} T_0^{b_2} = D_{X;m}(T_0) = \tilde{D}^{\varnothing}_X \tag{4}$$

where $\tilde{D}^{\varnothing}_X$ denotes the critical domain width. Whereby we have

$$T_0 = (a^{\varnothing}_{X;1} | a^{\varnothing}_{X;2})^{\frac{1}{b_2 - b_1}} \tag{5}$$

$$\tilde{D}^{\varnothing}_X = [(a^{\varnothing}_{X;1})^{b_2} (a^{\varnothing}_{X;2})^{-b_1}]^{\frac{1}{b_2 - b_1}}. \tag{6}$$

Equation (5) is valid for any $\varnothing$, thus it may serve as a means of checking the numerical values (3) read directly from the plots. It is easily verified that for each pair of coefficients (2) and (3) the same adequately conformable result is obtained:

$$T_0 \cong 4 \times 10^{-2}\ \mathrm{cm} = T_0^{\mathrm{FeSi}}. \tag{7}$$

This result agrees with the data of [4, 6]. For the critical widths (6) the values of (2) and (3) give

$$\tilde{D}^0_{SL} = 36, \quad \tilde{D}^{20}_{SL} = 43, \quad D^{30}_{SL} = 52, \quad \tilde{D}^{40}_{SL} = 60 \tag{8}$$

in 10^{-4} cm units. An adequate check of the correctness of readings (3) is the constancy of the ratio

$$a^{\varnothing}_{SL;1} / a^{\varnothing}_{SL;2} \cong 0.276\ \mathrm{cm}^{0.4} \tag{9}$$

the value of which is also in agreement with the result obtained in [4, 6]. Hence, by placing the values (2) and (3) into Eq. (1) we get for the *SL* domain structure in rectangular-prism-shaped FeSi samples of the orientations ⌀ under study the following dependences of domain width D upon effective crystal thickness T along the magnetically preferred direction:

$$D^{0}_{SL;1} = 0.0183T^{0.5}, \quad D^{20}_{SL;1} = 0.0220T^{0.5}$$
$$D^{30}_{SL;1} = 0.0265T^{0.5}, \quad D^{40}_{SL;1} = 0.0304T^{0.5} \tag{10}$$

for $T \leqslant T_0$, and

$$D^{0}_{SL;2} = 0.064T^{0.9}, \quad D^{20}_{SL;2} = 0.076T^{0.9}$$
$$D^{30}_{SL;2} = 0.093T^{0.9}, \quad D^{40}_{SL;2} = 0.110T^{0.9} \tag{11}$$

for $T \geqslant T_0$, where T and D are measured in cm. Proceeding analogously we get for the $D_{NC}(\varnothing = 45°)$ curve

$$b_1 = 0.3, \quad a_{NC;1} = 0.0103 \tag{12}$$

for $m = 1$ $(T \leqslant T_0)$, and

$$b_2 = 1.4, \quad a_{NC;2} = 0.201 \tag{13}$$

for $m = 2$ $(T \geqslant T_0)$, where the coefficient $a_{NC;m}$ is measured in cm^{1-b_m} units. The critical domain width and critical thickness for this structure are, in 10^{-4} cm units,

$$\tilde{D}_{NC} = 60, \quad T_0^{NC} = 840. \tag{14}$$

Hence, in agreement with Eqs (12) to (14) the law expressed in Eq. (1) takes the following form for the *NC* domain structure:

$$D_{NC;1} = 0.0103\, T^{0.3} \quad \text{for } T \leqslant T_0 \tag{15}$$

and

$$D_{NC;2} = 0.201\, T^{1.4} \quad \text{for } T \geqslant T_0 \tag{16}$$

where D and T are measured in cm.

It must be pointed out, however, that in the case of the *NC* domain structure for thicknesses t smaller than the spacing between 90° Bloch walls (α) there appear regions (which grow when t decreases) which contain an increasingly growing number of equidistant 180° Bloch walls (region *c* in Fig. 6). To differentiate between the cases, the domain width in these regions is denoted by D^{45}_{SL} instead of D_{NC}. Measurements show that D^{45}_{SL} depends on T just the same as D_{SL} for $0 \leqslant \varnothing \leqslant 45°$ (*i. e.* the same b_1, b_2 and T_0). This is seen by comparing the appropriate curves in Fig. 11. Therefore, in the case when $\varnothing = 45°$ we must differentiate between D^{45}_{SL} for the equidistant domain structure (Figs 3d and 5c) and D_{NC} for the structure at the edges (Figs 5a, d and 6a, d).

3.2. Wedge-shaped samples

The powder patterns in Figs 8 and 9 are examples of typical domain structures observed on the (100) surfaces of Fe−3.25% Si single crystals cut in the form of wedges according to the model of Fig. 1b. The samples of Fig. 8 differ by the cutting mode from those of Fig. 9. Namely, the former are crystallographically non-symmetrical with angles of $\vartheta = 0$ and $\theta = 18°$ (Fig. 8a) and $\vartheta = 5°$ and $\theta = 45°$ (Fig. 8b), whereas the other

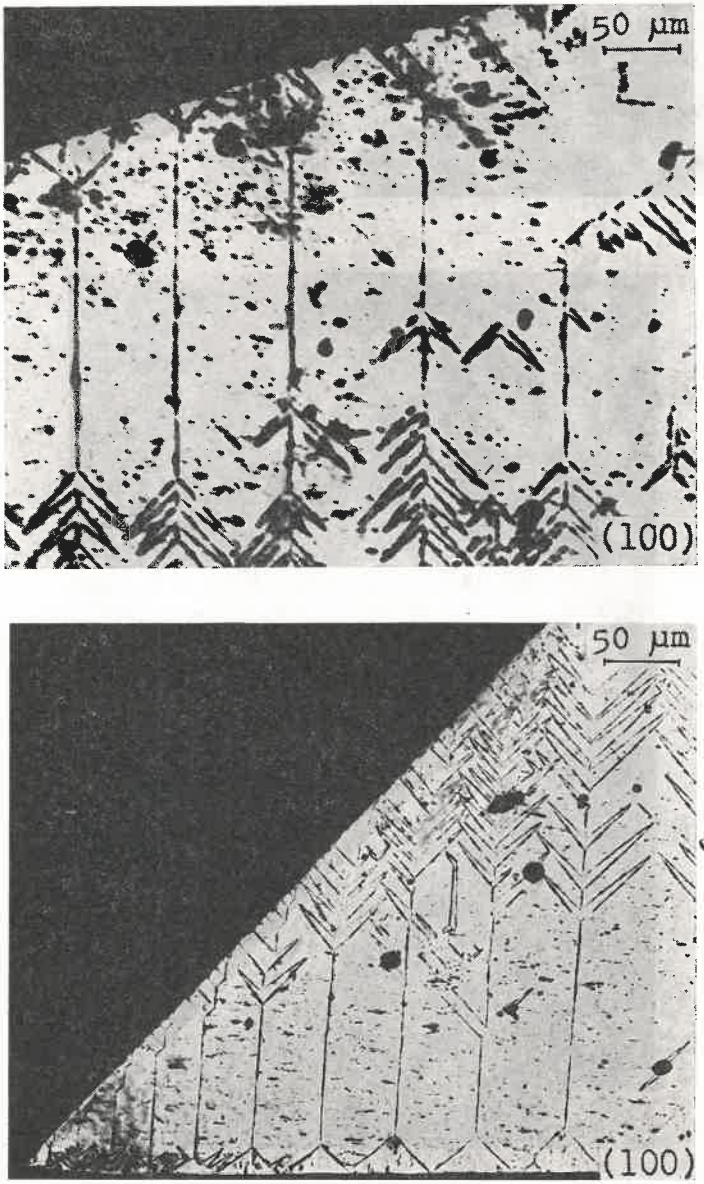

Fig. 8. Powder patterns on (100) lateral face for: a) $\vartheta = 0$ and $\theta = 18°$; b) $\vartheta = 5°$ and $\theta = 45°$

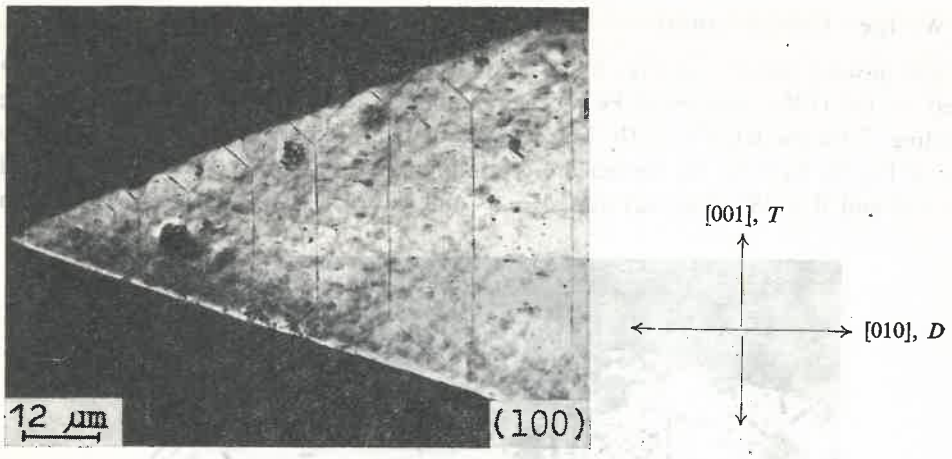

a

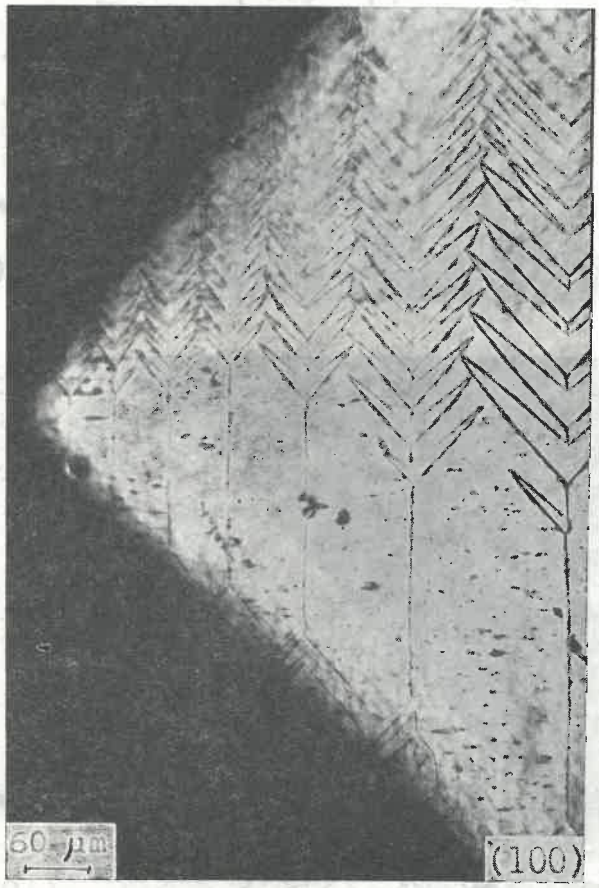

b

Fig. 9. Powder patterns on (100) lateral face for: a) $\vartheta = \theta = 20°$; b) $\vartheta = \theta = 45°$

samples are crystallographically (hence, magnetically) symmetrical, with $\vartheta = \theta = 20°$ (Fig. 9a) and $\vartheta = \theta = 45°$ (Fig. 9b).

It must be emphasized that the wedge-shaped sample of Fig. 9b is the cut-off edge (*a*) of the rectangular-prism-shaped sample of Figs 5 and 6 corresponding to $\varnothing = 45°$.

The examples of *SL* domain structure in Figs 8 and 9 have been so selected that they simultaneously correspond to various wedge angles of the samples, namely: $\vartheta + \theta = 18°$ (Fig. 8a), 40° (Fig. 9a), 50° (Fig. 8b) and 90° (Fig. 9b). The $D(T)$ curves or experimental

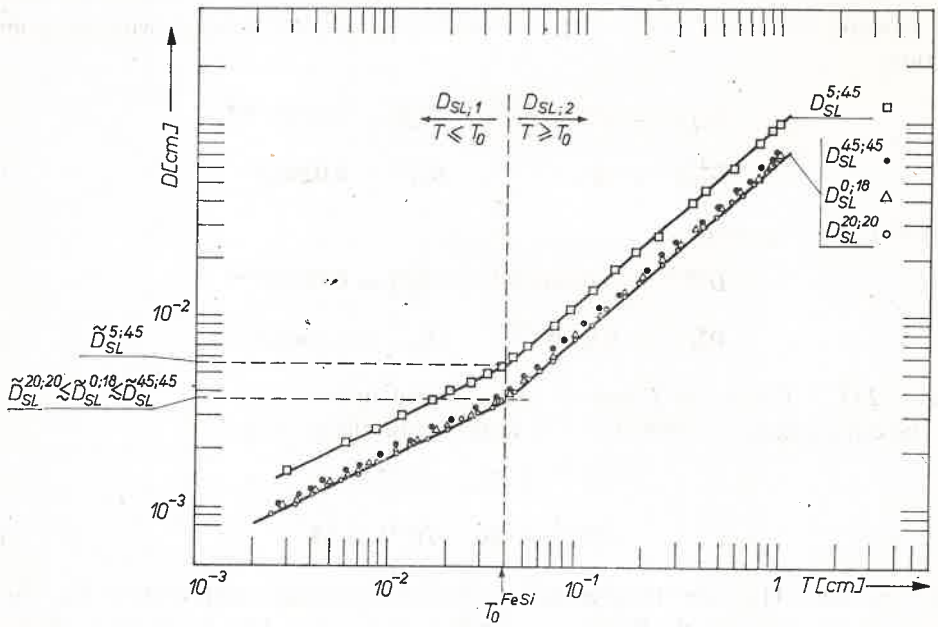

Fig. 10. Domain width D *versus* crystal thickness T for simple domain structure of single-crystalline Fe–3.25% Si samples in the form of wedges for: $\vartheta = \theta = 20°$ (curve $D_{SL}^{20;20}$), $\vartheta = 0°$ and $\theta \leqslant 18°$ (curve $D_{SL}^{0;18}$), $\vartheta = 5°$ and $\theta = 45°$ (curve $D_{SL}^{5;45}$)

points corresponding to these structures are shown in Fig. 10, the notation being $D_{SL}^{\vartheta;\theta}$. Readings from large plots give the values

$$b_1 = 0.5, \quad b_2 = 0.9, \quad T_0 = 4 \times 10^{-2}\ \text{cm} \tag{17}$$

for all of the curves, these values being in agreement with the results obtained for the *SL* structure with the use of the rectangular-prism-shaped samples with $0 \leqslant \varnothing < 45°$ (compare Fig. 7 and Eqs (2), (3) and (7)). Readings give the following values for the coefficients $a_{SL;m}^{\vartheta;\theta}$:

$$a_{SL;1}^{20;20} = 0.0186, \quad a_{SL;1}^{0;18} = 0.0190$$

$$a_{SL;1}^{45;45} = 0.0205, \quad a_{SL;1}^{5;45} = 0.0290 \tag{18}$$

for $m = 1$ ($T \leqslant T_0$), and

$$a_{SL;2}^{20;20} = 0.0660, \quad a_{SL;2}^{0;18} = 0.0680$$
$$a_{SL;2}^{45;45} = 0.0705, \quad a_{SL;2}^{5;45} = 0.1040 \tag{19}$$

for $m = 2$ ($T \geqslant T_0$), in units of cm^{1-b_m}.

It is simple to check that the quotients $a_{SL;1}^{\vartheta,\theta}/a_{SL;2}^{\vartheta;\theta}$ of coefficients (18) and (19) satisfy the equality (9) with satisfactory accuracy.

Put into Eq. (1), the data above lead to the following dependences of domain width D upon effective thicknesses T for the examined wedge-shaped samples with SL domain structure:

$$D_{SL;1}^{20;20} = 0.0186T^{0.5}, \quad D_{SL;1}^{0;18} = 0.0190T^{0.5}$$
$$D_{SL;1}^{45;45} = 0.0205T^{0.5}, \quad D_{SL;1}^{5;45} = 0.0290T^{0.5} \tag{20}$$

for $m = 1$ ($T \leqslant T_0$), and

$$D_{SL;2}^{20;20} = 0.0660T^{0.9}, \quad D_{SL;2}^{0;18} = 0.0680T^{0.9}$$
$$D_{SL;2}^{45;45} = 0.0705T^{0.9}, \quad D_{SL;2}^{5;45} = 0.1040T^{0.9} \tag{21}$$

for $m = 2$ ($T \geqslant T_0$), where T and D are measured in cm.

The critical domain widths for $T = T_0$ read from the plots are

$$\tilde{D}_{SL}^{20;20} = 37, \quad \tilde{D}_{SL}^{0;18} = 38$$
$$\tilde{D}_{SL}^{45;45} = 40, \quad \tilde{D}_{SL}^{5;45} = 58 \tag{22}$$

in 10^{-4} cm units. They are in agreement with those computed according to Eq. (6).

Let us note yet that the fir-like closure domains seen in Figs 8 and 9b (and also in Figs 3c and 5a, d) are the result of deviation of the lateral side of the sample from the (100) plane. Figures 3d, 5d and 8b also exhibit Néel type closure domains which form at larger crystal defects.

4. Concluding remarks

The experimental results obtained in this study are illustrated by the comprehensive plots in Fig. 11 and the Tables I and II which for clarity contain the data for only some of the samples selected in such a way as to be able to indicate certain general regularities characterizing the effect of the factors under study on the $D(T)$ dependence.

We must remember that the primary aim of this work was to verify the measurements of [4] made for the SL structure on an Fe–3.25% Si single-crystalline sample in the form of a wedge. It was to show whether — as for the ML structure [6] — the results obtained thus coincide with those obtained with the use of a series of rectangular-prism-shaped samples of various thicknesses along the magnetically preferred direction. According to the introduced terminology, the sample used in [4] was a "one-sided" wedge ($\vartheta = 0$),

hence, asymmetric to the extreme, while the wedge angle $(\vartheta+\theta)$ was 20°. Therefore, the results of [4] correspond with the results obtained here for the wedge-shaped sample having angles $\vartheta = 0$ and $\theta = 18°$ (second column of Table II). As is seen from the data of the first columns of Table I and II these results indeed differ but slightly from those obtained from the measurements on rectangular-prism-shaped samples of orientation $\varnothing = 0$ (the $D_{SL}^{0;18}$ curve for the wedge lies somewhat above the D_{SL}^{0} curve; compare Fig. 11). Thus, the results of our research are analogous as for the *ML* structure [6] in this respect.

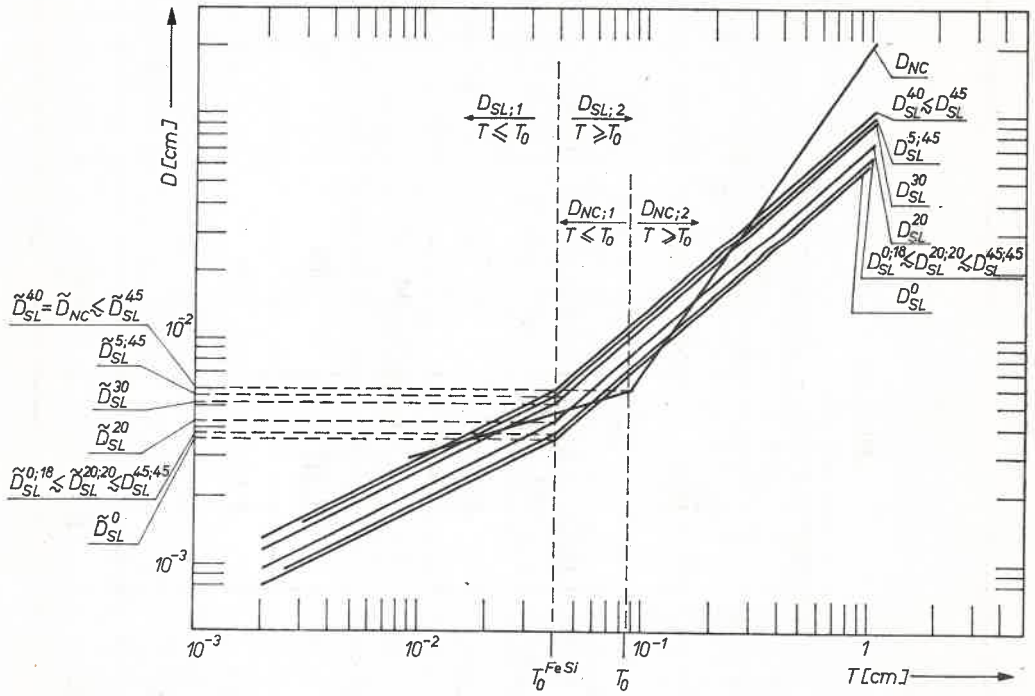

Fig. 11. Comprehensive curves of relation between domain width D and crystal thickness T of examined samples having the shape of rectangular-prisms and wedges for the simple (*SL*) Landau-Lifshitz domain structure in Fe−3.25% Si

The second goal of this study was to examine the effect of the wedge angle of wedge-shaped samples and their crystallographical orientation (manner of cutting) on the $D(T)$ curve. It is evident from Table II and the curves of Fig. 11 that:

1. at a fixed wedge angle $\vartheta+\theta$ the curve lies higher when the wedge is more asymmetrical, *i.e.* the more the angles ϑ and θ differ, and

2. at a fixed ratio of the angles ϑ and θ the curve lies higher when the wedge angle $\vartheta+\theta$ is larger.

The tables and curves also show that even at a larger wedge angle $\vartheta+\theta$ the $D(T)$ curve only slightly overlies the analogical curve for the rectangular-prism-shaped sample of orientation $\varnothing = 0$ if the wedge-shaped sample is symmetrical crystallographically, *i.e.*, if $\vartheta = \theta$ (compare, *e.g.*, the D_{SL}^{0} and $D_{SL}^{45;45}$ curves in Fig. 11).

Table I

Landau - Lifshitz domain structure	SL								NC	
Critical crystal thickness T_0	400 μm								840 μm	
Declination ϕ	Rectangular – prism – shaped samples									
	0°		20°		30°		40°		45°	
Crystal thickness T	$T \leq T_0$ $(m=1)$	$T \geq T_0$ $(m=2)$	$T \leq T_0$ $(m=1)$	$T \geq T_0$ $(m=2)$	$T \leq T_0$ $(m=1)$	$T \geq T_0$ $(m=2)$	$T \leq T_0$ $(m=1)$	$T \geq T_0$ $(m=2)$	$T \leq T_0$ $(m=1)$	$T \geq T_0$ $(m=2)$
Exponent b_m	0.5	0.9	0.5	0.9	0.5	0.9	0.5	0.9	0.3	1.4
Coefficient $a^{\phi}_{SL;m}$ $[cm^{1-b_m}]$	0.0183 $cm^{0.5}$	0.064 $cm^{0.1}$	0.022 $cm^{0.5}$	0.076 $cm^{0.1}$	0.0265 $cm^{0.5}$	0.093 $cm^{0.1}$	0.0304 $cm^{0.5}$	0.110 $cm^{0.1}$	0.0103 $cm^{0.7}$	0.201 $cm^{-0.4}$
Critical domain width $\tilde{D}^{\phi}_{SL} = \tilde{D}^{\phi}_{SL}(T_0) = a_{SL;m} T_0^{b_m}$	36 μm		43 μm		52 μm		60 μm		60 μm	
$a^{\phi}_{SL;1} / a^{\phi}_{SL;m} = T^{b_2 - b_1}$ $[cm^{b_2-b_1}]$	0.276 $cm^{0.4}$								0.051 $cm^{1.1}$	
$a^{\phi}_{SL;1} / a^{0}_{SL;2} = \tilde{D}^{\phi}_{SL} / \tilde{D}^{0}_{SL}$	1		1.20		1.45		1.66		———	
$a^{\phi}_{SL;m} / a^{20}_{SL;m} = \tilde{D}^{\phi}_{SL} / \tilde{D}^{20}_{SL}$	0.84		1		1.21		1.40		———	
$a^{\phi}_{SL;m} / a^{30}_{SL;m} = \tilde{D}^{\phi}_{SL} / \tilde{D}^{30}_{SL}$	0.69		0.83		1		1.16		———	
$a^{\phi}_{SL;m} / a^{40}_{SL;m} = \tilde{D}^{\phi}_{SL} / \tilde{D}^{40}_{SL}$	0.60		0.72		0.87		1		———	

Table II

Landau - Lifshitz domain structure		SL							
Critical crystal thickness T_0		400 μm							
Angles		Wedge - shaped samples							
	ϑ	20°		0°		45°		5°	
	Θ	20°		18°		45°		45°	
Crystal thickness T		$T \leqslant T_0$ $(m=1)$	$T \geqslant T_0$ $(m=2)$	$T \leqslant T_0$ $(m=1)$	$T \geqslant T_0$ $(m=2)$	$T \leqslant T_0$ $(m=1)$	$T \geqslant T_0$ $(m=2)$	$T \leqslant T_0$ $(m=1)$	$T \geqslant T_0$ $(m=2)$
Exponent b_m		0.5	0.9	0.5	0.9	0.5	0.9	0.5	0.9
Coefficient $a_{SL;m}^{\vartheta;\Theta}$ $[cm^{1-b_m}]$		$0.0186\,cm^{0.5}$	$0.0660\,cm^{0.1}$	$0.0190\,cm^{0.5}$	$0.0680\,cm^{0.1}$	$0.0205\,cm^{0.5}$	$0.0705\,cm^{0.1}$	$0.0290\,cm^{0.5}$	$0.1040\,cm^{0.1}$
Critical domain width $\tilde{D}_{SL}^{\vartheta;\Theta} = \tilde{D}^{\vartheta;\Theta}(T_0) = a_{SL;m}^{\vartheta;\Theta} T_0^{\,b_m}$		37 μm		38 μm		40 μm		58 μm	
$a_{SL;1}^{\vartheta;\Theta} / a_{SL;2}^{\vartheta;\Theta} = T^{b_2-b_1}$ $[cm^{b_2-b_1}]$		$0.276\,cm^{0.4}$							
$a_{SL;m}^{\vartheta;\Theta} / a_{SL;m}^{20;20} = \tilde{D}_{SL}^{\vartheta;\Theta} / \tilde{D}_{SL}^{20;20}$		1		1.03		1.1		1.57	
$a_{SL;m}^{\vartheta;\Theta} / a_{SL;m}^{0;18} = \tilde{D}_{SL}^{\vartheta;\Theta} / \tilde{D}_{SL}^{0;18}$		0.97		1		1.05		1.53	
$a_{SL;m}^{\vartheta;\Theta} / a_{SL;m}^{45;45} = \tilde{D}_{SL}^{\vartheta;\Theta} / \tilde{D}_{SL}^{45;45}$		0.94		0.96		1		1.47	
$a_{SL;m}^{\vartheta;\Theta} / a_{SL;m}^{5;45} = \tilde{D}_{SL}^{\vartheta;\Theta} / \tilde{D}_{SL}^{5;45}$		0.64		0.95		0.69		1	

On the other hand, for extremely asymmetrical wedge-shaped samples ($\vartheta = 0$) the difference of domain widths for large T may be very pronounced (*e.g.*, it is almost 60% at $T = 1$ cm; compare D_{SL}^{0} and $D_{SL}^{5;45}$ curves in Fig. 11). It follows thus that wedge-shaped samples of symmetrical orientation ($\vartheta = \theta$) are the most suitable for $D(T)$ measurements.

The third aim of this paper was to show the effect of the orientation of a rectangular-prism-shaped sample on the $D(T)$ curve. Table I and the curves of Fig. 11 demonstrate that for the same domain structure the $D(T)$ curve lies higher when the angle Φ is larger, *i.e.*, when the angle between the top (and bottom) crystal face and the Bloch walls separating the main domains is smaller. In this case also, the differences in domain widths may be considerable for large effective thicknesses T (*e.g.*, for the D_{SL}^{0} and D_{SL}^{40} curves this difference amounts to over 70% at $T = 1$ cm; see Fig. 11).

The results found in the present work and those of [6, 7] show that domain width measurements on single crystals of random shape, crystallographic orientation and dimensions do not ensure that a proper $D(T)$ curve, as regards both the coefficients $a_{X;m}$ and the exponents b_m in Eq. (1), will be determined even though the domain structure may be exactly known. Our studies also supply further proof that [3, 4] lead to the correct conclusion that the exponent b_2 for $T > T_0$ and the critical thickness T_0 depend solely on the material. On the other hand, our investigation and those of [6, 7] clearly show that the coefficients $a_{X;m}$ depend not only on the material and domain structure type, but also on the shape and crystallographic orientation of the sample. From a more general point of view, that the last two factors affect the $D(T)$ curve is rather obvious because, strictly speaking, they bring about a change of the domain structure, since they change the shape (and sometimes even the type) of the closure domains.

This rule is distinctly disobeyed by the $D_{NC}(T)$ curve of Figs 7 and 11. It differs from the other curves by the exponents b_1 and b_2 and the critical thickness T_0 (last column of Table I) alike. This fact may be explained, however, when it is considered that the domain structure corresponding to this curve constitutes a sort of closure structure for the main (equidistant) *NC* domain structure (region *c* in Fig. 6) to which, in turn, corresponds the D_{SL}^{45} curve in Fig. 11 practically tyllying with the D_{SL}^{40} curve (see comments following Eq. (16)). This is corroborated by the fact that sample thickness t bears no effect on the $D_{NC}(T)$ curve (see Fig. 6). Also, this structure obeys the general law when it constitutes the main domain structure of the sample (compare Fig. 9b and the $D_{SL}^{45;45}$ curve in Figs 10 and 11). In addition, this effect demonstrates the inadequacy of the $D(T)$ measurements described in [12], even had they been performed with greater accuracy.

The author is grateful to Dr B. Wysłocki and Dr W. J. Ziętek for helpful advice during the performance of this work.

REFERENCES

[1] L. D. Landau, E. Lifshitz, *Phys. Z. Sov.*, **8**, 153 (1935).
[2] H. J. Williams, R. M. Bozorth, W. Shockley, *Phys. Rev.*, **75**, 155 (1949).
[3] B. Wysłocki, W. J. Ziętek, *Phys. Letters*, **29A**, 114 (1969).
[4] B. Wysłocki, *Acta Phys. Polon.*, **35**, 731 (1969).
[5] B. Wysłocki, *Acta Phys. Polon.*, **34**, 327 (1968); **35**, 179 (1969).

[6] S. Szymura, B. Wysłocki, W. J. Ziętek, *Acta Phys. Polon.*, **A38**, 405 (1970).
[7] S. Szymura, *Acta Phys. Polon.*, **A41**, 43 (1972).
[8] L. Néel, *Cahiers Phys.*, **25**, 1, 24 (1944); *J. Phys. Radium*, **17**, 250 (1956).
[9] G. Sołtysik, B. Wysłocki, *Prace Inst. Hutniczych*, **19**, 247 (1967) (Polish, English and Russian summary).
[10] W. C. Elmore, *Phys. Rev.*, **51**, 982 (1937); **53**, 757 (1938).
[11] J. R. Garrood, *Proc. Phys. Soc.*, **A79**, 1252 (1962).
[12] C. G. Graham, P. W. Neurath, *J. Appl. Phys.*, **28**, 888 (1957).